

# Handling stability analysis of decoupling suspension for formula racing

Han XU<sup>1b\*</sup>, Jiachuan XU, Xuemin CUI, Yang ZHOU, Xinyu SUN, and Zongqi WANG

Shandong University of Technology, China

**Abstract.** In this paper, a university formula racing suspension is taken as the research object. Based on the requirements of racing suspension, the double wishbone suspension is improved, and a new arrangement scheme based on the stepped shaft is proposed, which theoretically realizes the decoupling of the pitch stiffness and the roll stiffness of the suspension. Based on the ADAMS/Car module, the front and rear suspension models are established. By simulating the motion of formula racing, it is further judged whether the pitch and roll stiffness of the suspension are decoupled. According to this, the hard point coordinates of the suspension are adjusted to ensure that the length of each spring changes within the ideal range. Based on the optimized suspension, according to the national standard test method and the scoring standard of the automobile industry, combined with the university formula racing project, the vehicle handling stability test and scoring evaluation are carried out, and the vehicle handling stability is verified by the real vehicle test. A set of decoupling suspensions is obtained, which can have pitch stiffness and roll stiffness separately adjusted, with improved vehicle handling stability.

**Keywords:** decoupling suspension; ADAMS/CAR; formula racing.

## 1. INTRODUCTION

Formula SAE of China (FSAE) is a car design and manufacturing event. The main participants are college students majoring in vehicle engineering and related fields. The participating teams are all composed of schools as units. Additionally, with the rapid development of the university formula racing competition, people have increasingly high requirements for the handling stability of the racing [1–3]. Most domestic and foreign fleets utilize the conventional suspension with double shock absorbers and lateral stabilizer bars, and the pitch and roll solution of the suspension is implemented by adding a third spring or a lateral stabilizer bar [4,5]. However, the adjustable upper limit of scheme suspension is relatively low, and the suspension mass is significantly increased, which is not conducive to improving the handling stability of the racing.

When it is the main springs on both sides that ensure the suspension pitch and roll stiffness of the racing, to improve its steady-state steering characteristics the spring stiffness needs to be increased to enhance the roll stiffness. However, as the pitch stiffness increases, the comfort of the ride deteriorates. Conversely, when the comfort of the ride is improved by reducing the spring stiffness to lower the pitch stiffness, the roll stiffness is reduced, leading to the deterioration of the racing steering characteristics.

To improve the suspension angle stiffness without affecting the suspension line stiffness, Sindhwan *et al.* proved that anti-roll bars can reduce the amplitude of body roll during wheel

turns and improve racing stability [6]. Kumar *et al.* discovered that adding anti-roll bars in suspension systems reduced the change in camber angle, which can enhance control cornering [7]. Javanshir *et al.* minimized suspension system camber angle variations by adding anti-roll bars and optimizing torsion bars [8]. Kelkar *et al.* investigated the importance of an anti-roll bar device to tune the car roll stiffness without interfering with the ride stiffness [9]. Ke Ma added lateral stabilizer bars to the front and rear air suspension systems. The results show that the comprehensive evaluation score of handling stability increased from 80.38 to 85.05, and the handling stability of the full vehicle improved [10]. To decouple suspension line stiffness and angular stiffness, some scholars proposed adding a third spring to provide additional line stiffness. Liu *et al.* explained the geometric design of the racing suspension and the calculation process of the stiffness of each spring after adding the third spring [11], while Shi *et al.* studied the working principle of adding a third spring and conducted a kinematic simulation [12]. Yang *et al.* of Wenzhou University designed a three-spring decoupling suspension to achieve the decoupling of suspension and adjust the pitch stiffness and roll stiffness separately [13]. Based on the double wishbone non independent suspension, Dongmei Wu *et al.* changed the hard point design of the spring position and adopted the geometric suspension layout form of one spring transversely placed and one spring oblique placed to realize the decoupling between the roll motion and pitch motion of the formula racing [14]. Shuanglu Quan *et al.* connected the rotating centers of the two shock absorbers to the frame through bearings and rotated the rotating shaft through the push rod to compress the shock absorber and inhibit the tendency of vehicle trim, resulting in the decoupling of suspension pitch stiffness and roll stiffness [15].

\*e-mail: 19806142195@163.com

Manuscript submitted 2024-07-04, revised 2025-01-21, initially accepted for publication 2025-02-03, published in May 2025.

The above analysis shows that the adjustable property of the double shock absorber and side stabilizer bar suspension is limited, the mass is increased, and the third spring design cannot completely achieve the decoupling of pitch and roll stiffness. Decoupling suspensions designed by some scholars lack evaluation through full vehicle simulation and real vehicle tests, and the improvement of vehicle handling stability by such design awaits verification. Therefore, a decoupling suspension design scheme is proposed in this paper. Two independent spring shock absorbers correspond to the trim and roll conditions, respectively, in theory achieving the decoupled pitch stiffness and roll stiffness. Based on the ADAMS/CAR module, a suspension dynamic model is established for simulation and optimization to assess the findings of the theoretical analysis. Finally, a real vehicle test is conducted to verify the improvement of handling stability of the full vehicle by the design.

To determine the impact of suspension on the handling and stability performance of the racing, most scholars use virtual simulation to study the overall performance of the racing [16]. Pridie and Antonya designed a formula racing suspension and conducted braking and acceleration simulation tests on the virtual model [17]. The vehicle performance was analyzed by Zhang *et al.*, with ADAMS/CAR used for contrast according to the evaluation index of minimum time handling and stability [18]. Kim *et al.* established a virtual prototype model of the suspension of a heavy truck. The key hard point coordinates of the suspension are taken as design variables to optimize the suspension characteristics [19]. To improve the suspension performance of the racing, Vlad *et al.* optimized the wheel alignment parameters by identifying hard point coordinates that had a significant impact on the optimization objectives [20]. Zhang *et al.* conducted a simulation of the vehicle dynamics model of the racing in the eight-shaped ring project, analyzing the performance of the racing on actual tracks [21]. Balena *et al.* conducted an acceleration, braking, and eight-shaped ring project based on the racing dynamics model to assess the overall handling stability of the racing [22]. However, certain subjective factors in the evaluation parameters of the test cannot better assess the overall performance of the racing.

To assess more objectively whether the relevant parameters of each test of the racing meet the requirements, most researchers refer to the Chinese vehicle handling stability test method to conduct simulation tests and evaluate them according to the Chinese vehicle handling stability index limit and evaluation method [23, 24]. Chai conducted kinetic simulation optimization on FSAE racing suspension based on ADAMS/CAR software and performed vehicle handling stability simulation and score evaluation [25]. Zhang conducted simulation tests such as the steady-state slewing test and snake-shaped test on FSAE racing and scored and evaluated each evaluation parameter [26]. The relevant researchers refer to the Chinese test method to test the FSAE racing, but the radius of the steady-state slewing test and the pile spacing of the snake-shaped test exceeds the radius and pile spacing of the racing competition project. The score obtained by the test can show that the vehicle meets the competition requirements, but the competition performance cannot be better assessed.

To better assess the performance of the racing, Zhou from Chang'an University proposed an index to evaluate the steady-state slewing test, i.e., the maximum lateral acceleration [27]. Large lateral acceleration means that the lateral limit performance of the vehicle is better, and the control stability of the full vehicle is also better. Qiao *et al.* from Chang'an University pointed out that racing with a large lateral acceleration could quickly pass through the splayed loop project with a turning radius of only 9.125 m [28]. Therefore, the maximum lateral acceleration is taken as the evaluation index of the steady-state slewing test. Yang and Hong proposed taking the maximum lateral acceleration as the evaluation index of the steady-state slewing test and determined the upper and lower limits of the scoring formula according to the results [29, 30].

The above analysis has significance for the handling stability evaluation of formula racing. This paper comprehensively considers the test methods of national standards, industry evaluation standards, and competition project requirements, using the maximum lateral acceleration, understeer degree, and body roll degree as the test evaluation indicators. In addition, the test standards are improved, difficulties are overcome, and the comprehensive score of the steady-state slewing test is calculated for a more comprehensive evaluation of the vehicle handling stability.

## 2. DECOUPLED SUSPENSION SCHEME AND DESIGN

The decoupled layout scheme is adopted for the suspension to solve the problem of pitch and roll stiffness being difficult to adjust, and the motion law of the suspension is analyzed. The workflow is shown in Fig. 1.

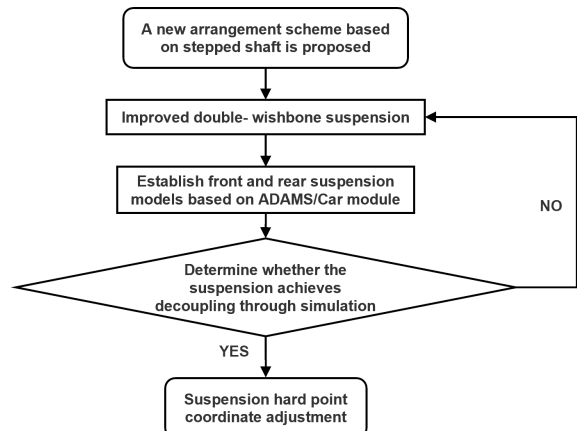


**Fig. 1.** Design and verification of decoupling suspension Workflow Diagram 1

### 2.1. Dynamic analysis of decoupling suspension layout scheme

#### (1) Layout scheme

The main components and arrangement scheme of decoupling suspension are shown in Fig. 2. Due to the approximate horizontal arrangement of the shock absorber in the FSAE racing suspension design, the small ground clearance of the racing, and

the low height of the whole vehicle, the rocker arm required for the connection between the shock absorber and the cross-arm is transformed into a stepped shaft, as shown in Fig. 2a and 2b. There are two rotating arms on one stepped shaft, and the connection points on the rotating arm connect with the push rod and two spring shock absorber assemblies, respectively. Both ends of the stepped shaft are fixed on the frame through the support.

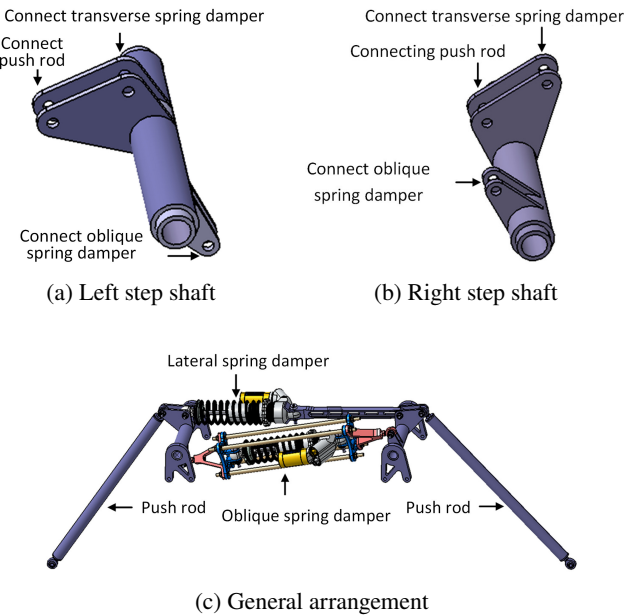


**Fig. 2.** Decoupling arrangement

## (2) Analysis of motion

When the racing is in pitch motion, push rods on both sides push the step shaft and rotate inward simultaneously. The distance between the two points connecting the lateral spring damper assembly on the ladder shafts on both sides diminishes. Therefore, the lateral spring damper assembly is compressed. While the step axis rotates inward simultaneously, the distance between the two points connecting the inclined spring damper assembly on the ladder shafts on both sides remains unchanged. Therefore, the inclined spring damper assembly is not compressed, as shown in Fig. 3a.

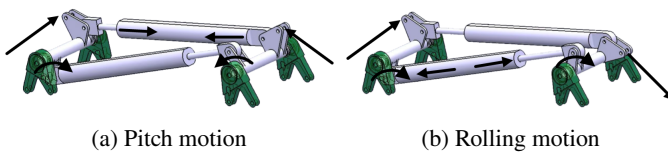


**Fig. 3.** Motion law of decoupling suspension

When the racing is in roll motion, push rods on both sides push the ladder shaft to rotate clockwise or counterclockwise simultaneously. The distance between the two points connecting the lateral spring damper assembly on the ladder shafts on both sides remains unchanged. Therefore, the lateral spring damper assembly is neither compressed nor extended. While the step

shaft rotates clockwise or counterclockwise simultaneously, the distance between the two points connecting the inclined spring damper assembly on the ladder shafts on both sides increases or decreases. Therefore, the inclined spring damper assembly is either compressed or stretched, as shown in Fig. 3b.

It can be seen from motion analysis that the length of the inclined spring damper assembly remains unchanged when the racing body is in pitching motion. The length of the lateral spring damper assembly remains the same when the racing body rolls, so the lateral springs provide the pitch stiffness of the suspension, and the inclined springs provide the roll stiffness of the suspension; decoupling of suspension pitch stiffness and roll stiffness is theoretically achieved.

## 2.2. Modeling and simulation analysis of decoupling suspension

The decoupling suspension model is established in the ADAMS/CAR module and assembled with the suspension test bench to obtain the simulation models of front and rear suspension test benches, as shown in Fig. 4.

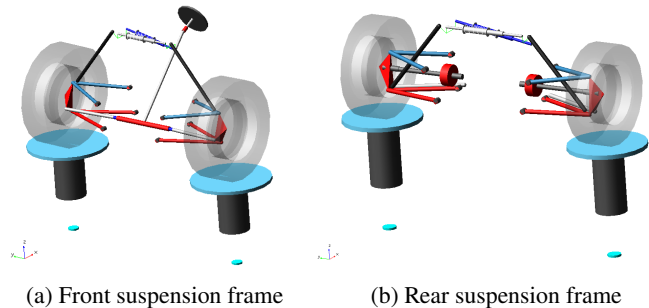
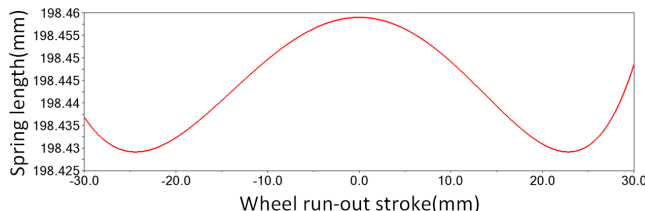


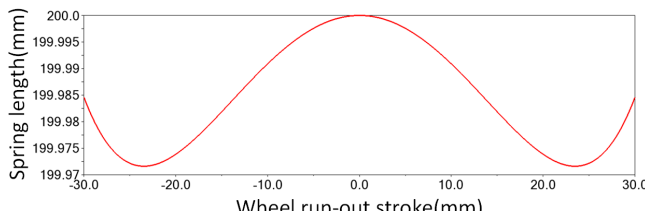
**Fig. 4.** Simulation model

The simulation of suspension is performed by inputting excitation to wheels. First, input the vertical run-out of the same size and direction to the left and right wheels of the same axle to simulate the wheel run-out caused by the car body when encountering obstacles or accelerating and decelerating. Next, enter the same but opposite vertical run-out to simulate the wheel run-out caused by the car turning. The lateral spring provides rigidity under the excitation of two wheels in the same direction. If the oblique spring does not work, the change of its length shall be as small as possible. Under the double-wheel reverse excitation, the inclined spring provides rigidity, the horizontal spring does not work, and the change of its length is as small as possible.

To further judge whether the decoupled suspension is completely decoupled, the front and rear suspensions are input with the excitation of two wheels in the same direction and the excitation of two wheels in the opposite direction. The wheel run-out range is [-30 mm, 30 mm]. Observe the spring length change that does not provide rigidity when the front and rear suspensions are jumping and optimize and adjust the hard point coordinates of the suspension according to the simulation results. Through continuous iterative calculation, the final spring length change curve that does not provide the rigidity is obtained, as shown in Figs. 5 and 6.



(a) Length of oblique spring when the double wheels bounce in the same direction

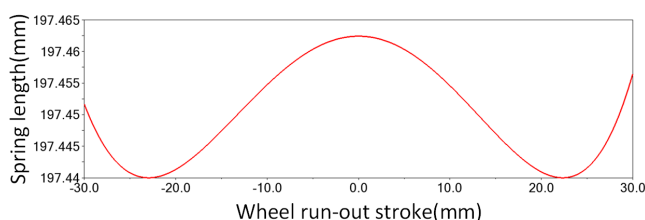


(b) Length of lateral spring when the double wheels bounce in the opposite direction

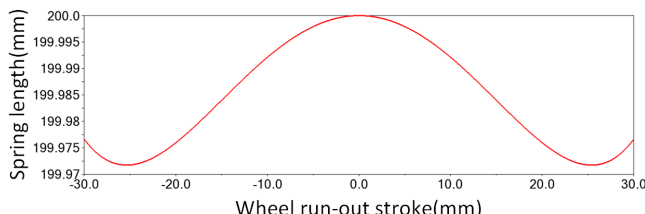
**Fig. 5.** Simulation curve of length change of front suspension spring

It can be seen from Fig. 5 that the length variation of the front suspension inclined spring is 0.06 mm under the excitation of double wheels in the same direction. Under the opposite direction excitation of double wheels, the length variation of the transversal spring is 0.04 mm, and the length variation of the spring is minimal.

It can be seen from Fig. 6 that the length variation of the inclined spring of the rear suspension is 0.04 mm under the excitation of double wheels in the same direction. Under the opposite direction excitation of double wheels, the length variation of the transversal spring is 0.06 mm, and the length variation of the spring is minimal.



(a) Length of oblique spring when the double wheels bounce in the same direction



(b) Length of lateral spring when the double wheels bounce in the opposite direction

**Fig. 6.** Simulation curve of length change of rear suspension spring

Analysis shows that the length change of the oblique spring is small under the same direction of double-wheel excitation, and the length change of the lateral spring is small under the opposite direction of double-wheel excitation. However, the wheel run-out in the actual competition is far lower than the simulated tire run-out, so the spring not providing stiffness exhibits a slight change, with achieved decoupling of pitch and roll stiffness.

### 2.3. Wheel alignment parameter selection and suspension geometry design

Based on the simulation results and the competition experience over the years, the wheel positioning parameters are selected [31], and the hard point size of the suspension geometry is designed.

#### (1) Selection of wheel alignment parameters

Wheel alignment parameters include camber angle, toe-in angle, kingpin inclination angle, and kingpin caster angle.

Wheel alignment parameters as shown in Table 1.

**Table 1**

Wheel alignment parameters

| Positioning parameters | Camber angle | Toe-in angle | Kingpin caster angle | Kingpin inclination angle |
|------------------------|--------------|--------------|----------------------|---------------------------|
| Front suspension frame | -1°          | -0.2°        | 3.52°                | 4°                        |
| Rear suspension frame  | -1°          | 0.1°         | 0                    | 0                         |

#### (2) Suspension geometry design

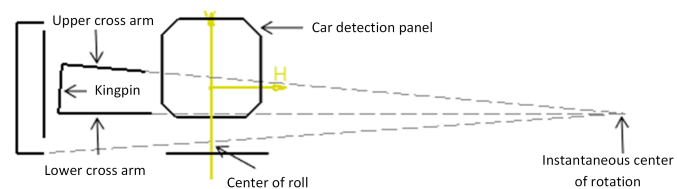
Based on the simulation results and the entry experience of the Shandong University of Technology in formula racing, the basic parameters for setting the suspension design are shown in Table 2.

**Table 2**

Basic parameters

| Wheelbase (mm) | Wheel track (mm) | Axle load ratio | Cross arm ratio | Offset frequency (Hz) | Height of center of mass (mm) |
|----------------|------------------|-----------------|-----------------|-----------------------|-------------------------------|
| 1560           | 1180             | 47:53           | 0.8             | 3.6                   | 320                           |

The front view of the front suspension is designed according to the geometric design knowledge of the vehicle suspension, as shown in Fig. 7. Hard point coordinates of front and rear suspensions are shown in Table 3 and Table 4.

**Fig. 7.** Front view geometry of the front suspension

**Table 3**  
Coordinates of initial hard point of front

| Name              |                                      | X        | Y        | Z       |
|-------------------|--------------------------------------|----------|----------|---------|
| hpl_bc            | Forward point of step axis           | 90.765   | -180     | 420     |
| hpl_bc2           | Rear point of step axis              | 10.765   | -180     | 420     |
| hpl_lca_front     | Front point of lower wishbone        | -150     | -200     | -88.075 |
| hpl_lca_outer     | Outer point of lower wishbone        | 0        | -549     | -92     |
| hpl_lca_rear      | Rear point of lower wishbone         | 150      | -200     | -88.075 |
| hpl_prod_inboard  | Push rod inner point                 | 10.765   | -215.3   | 454.8   |
| hpl_prod_outboard | External point of push rod           | 10.765   | -501.763 | 100     |
| hpl_tierod_inner  | Inner point of steering tie rod      | -29.0031 | -219.933 | -61.7   |
| hpl_tierod_outer  | Outer point of steering tie rod      | -58.579  | -545     | -57.53  |
| hpl_uca_front     | Front point of upper wishbone        | 139.235  | -240.77  | 50.231  |
| hpl_uca_outer     | Outer point of upper wishbone        | 10.765   | -536.763 | 83      |
| hpl_uca_rear      | Rear point of upper wishbone         | 160.765  | -240.77  | 50.231  |
| hpl_wheel_center  | Wheel core point                     | 0        | -595     | 0       |
| hps_roll_1        | Left point of oblique spring damper  | 90.765   | -172     | 387.7   |
| hps_roll_2        | Right point of oblique spring damper | 90.765   | 172      | 454.4   |
| hps_trim_left.y   | Left point of lateral spring damper  | 10.765   | -172.9   | 452     |
| hps_trim_right.y  | Right point of lateral spring damper | 10.765   | 172.9    | 452     |

**Table 4**  
Coordinates of initial hard point of rear

| Name                |                                      | X    | Y        | Z       |
|---------------------|--------------------------------------|------|----------|---------|
| hpl_bc              | Forward point of step axis           | 1605 | -200     | 210     |
| hpl_bc2             | Rear point of step axis              | 1525 | -200     | 210     |
| hpl_drive_shaft_inr | Drive axle shaft output point        | 1560 | -200.66  | 0       |
| hpl_lca_front       | Front point of lower wishbone        | 1450 | -225.23  | -86.621 |
| hpl_lca_outer       | Outer point of lower wishbone        | 1525 | -523     | -93     |
| hpl_lca_rear        | Rear point of lower wishbone         | 1640 | -225.23  | -86.621 |
| hpl_prod_inboard    | Push rod inner point                 | 1525 | -235     | 240     |
| hpl_prod_outboard   | External point of push rod           | 1525 | -500     | -73     |
| hpl_tierod_inner    | Inner point of lower pull rod        | 1690 | -225.23  | -86.621 |
| hpl_tierod_outer    | Outer point of lower pull rod        | 1575 | -523     | -93     |
| hpl_uca_front       | Front point of upper wishbone        | 1440 | -270.32  | 57.559  |
| hpl_uca_outer       | Outer point of upper wishbone        | 1555 | -517.098 | 76      |
| hpl_uca_rear        | Rear point of upper wishbone         | 1670 | -270.32  | 57.559  |
| hpl_wheel_center    | Wheel core point                     | 1560 | -585     | 0       |
| hps_roll_1          | Left point of oblique spring damper  | 1605 | -195.4   | 175.4   |
| hps_roll_2          | Right point of oblique spring damper | 1605 | 195.4    | 242.6   |
| hps_trim_left       | Left point of lateral spring damper  | 1525 | -199.5   | 242.8   |
| hps_trim_right      | Right point of lateral spring damper | 1525 | 199.5    | 242.8   |

### 3. ESTABLISHMENT OF FULL VEHICLE MODEL

Based on the ADAMS/CAR module, the assembly models of front suspension, steering, tire, body, power, and brake subsystem are simulated and analyzed to reflect the racing performance in actual operation better.

#### 3.1. Steering subsystem

For the racing, a rack-and-pinion steering system and ADAMS/CAR software steering system template are adopted. The rack angular transmission ratio is set as 0.078 rad/m, corresponding parameters are modified, each node hard point co-

ordinates are adjusted, and the steering subsystem based on the template in the standard mode is generated.

### 3.2. Tire subsystem

The tires used by the Shandong University of Technology every year are Hoosier hot-melt tires, which have an excellent grip. The tire system template of ADAMS/CAR software is used to modify the tire geometry and relevant parameters and generate the tire subsystem based on the template.

### 3.3. Body subsystem

In the actual body system, there are many mechanical parts, the establishment of the model is more complex, and the complex vehicle body system is simplified into a spherical object. This paper mainly studies the influence of suspension systems on vehicle handling stability, so the influence of air on the kinematic model is ignored. The spherical automobile body subsystem of ADAMS/CAR software is adopted. It adds vehicle body location information, quality information, communicator information, etc., and generates the vehicle body subsystem based on the template.

### 3.4. Power assembly and brake subsystem

In ADAMS/CAR software, the power system is different from other models because there is no need to establish a real model. Instead, external characteristic curve of an engine of the racing and transmission ratios at all levels of the transmission are edited into the property file of the power module in the setting, data, and mathematical functions simulate the powertrain to drive the vehicle movement. The brake system is also set by setting parameters such as braking force and friction area.

### 3.5. Full vehicle model

In standard mode, each subsystem is assembled into a full vehicle simulation model through assembly and test stand, as shown in Fig. 8, to properly match the suspension with the vehicle, ob-

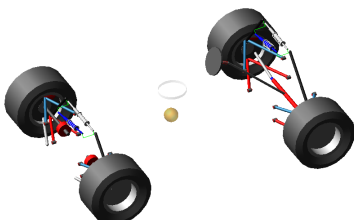


**Fig. 8.** Full vehicle model

taining the racing vehicle parameters is necessary. The vehicle parameters measured are shown in Table 5.

## 4. SIMULATION AND EVALUATION OF VEHICLE HANDLING STABILITY TEST

By GB/T6326-2014 Automobile Handling Stability Test Method (2014) and QC/T 480-1999 Limits and Evaluation Methods of Automobile Handling Stability Index (1999) and in combination with the University Formula Racing Project, the vehicle is subjected to the steady-state slewing test, snaking test and scoring evaluation. The workflow is shown on Fig. 9.

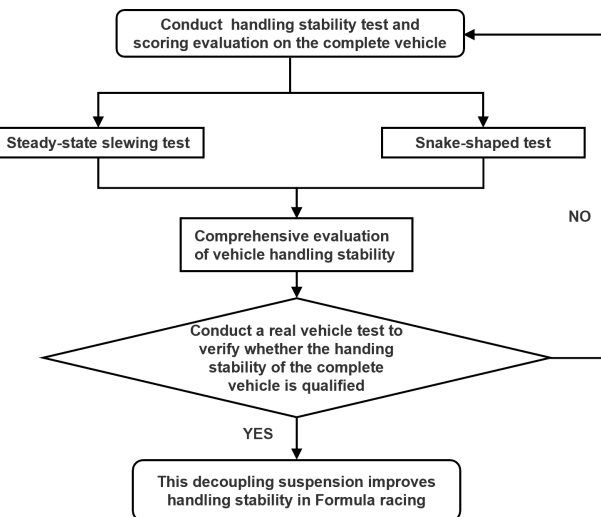


**Fig. 9.** Simulation and evaluation of vehicle handling stability test Workflow diagram 2

### 4.1. Steady-state slewing test

The steady-state slewing test assesses the stability and control performance of the vehicle and analyzes whether the car is stable under the steering input.

The figure of the eight-shaped ring project in the FSAE competition is similar to the steady-state slewing test, but its turning radius is far lower than 15 m in the national standard steady-state slewing test. In this paper, according to the national standard and the actual situation of the FSAE race, the steady-state slewing test of the car is conducted, so that the car runs along a circle with a radius of 9.125 m. Therefore, the final score of the

**Table 5**  
Basic parameters of full vehicle

| Parameter name         | Parameter value | Parameter name                                      | Parameter value |
|------------------------|-----------------|---|-----------------|
| Total length (mm)      | 3001            | Curb weight (kg)                                    | 240             |
| Total width (mm)       | 1417            | Quality of driver (kg)                              | 70              |
| Total height (mm)      | 1190            | Height of center of mass (mm)                       | 300             |
| Wheelbase (mm)         | 1580            | Axle load ratio                                     | 47:53           |
| Front wheel track (mm) | 1190            | Distance between center of mass and front axle (mm) | 826.8           |
| Rear wheel track (mm)  | 1170            | Distance between center of mass and rear axle (mm)  | 733.2           |

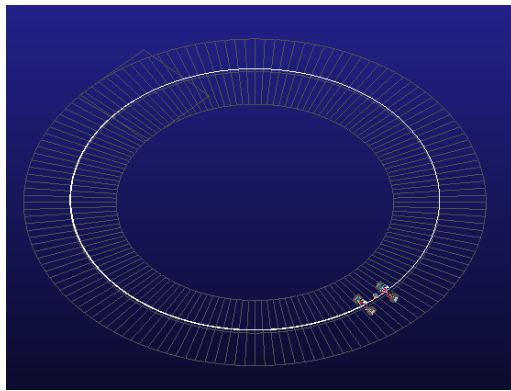
steady-state slewing test is lower than that of the test with a radius of 15 m.

### (1) Steady-state slewing test method

The racing runs at 10 km/h (minimum stable speed) along the circumference with a radius of 9.125 m. The vehicle is driven along the circumference by continuously adjusting the steering wheel angle, and the speed is gradually increased until the maximum lateral acceleration is reached (the maximum lateral acceleration of the vehicle is 1.03 g through multiple tests). The whole test process is recorded.

### (2) Steady-state slewing test setup and simulation results

In the vehicle simulation of the ADAMS/CAR software module, select the turning test with the radius unchanged, set relevant parameters according to the test method, and allow the vehicle to shift gears. The simulation duration is 15 s, and the simulation path is shown in Fig. 10.



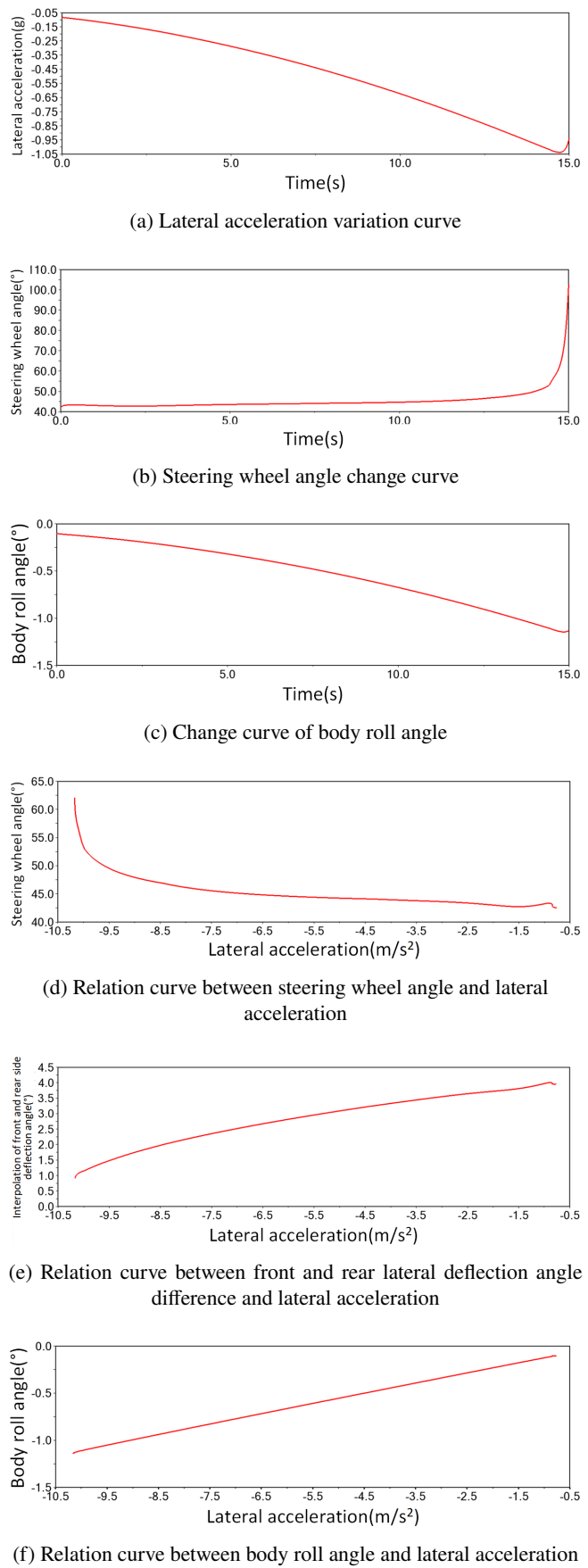
**Fig. 10.** Roadmap of steady-state slewing test track

Figure 11a–11c shows the steady-state slewing test simulation results. Based on the test data, the relation curve between the steering wheel angle, the difference between the front and rear axle lateral deflection angles, and the lateral acceleration of the body can be obtained, as shown in Fig. 11d–11f, it provides the basis for the corresponding scoring evaluation formula.

Figure 11d shows that the lateral acceleration increases from  $-0.9 \text{ m/s}^2$  to  $-9.7 \text{ m/s}^2$ . To maintain a pre-determined path, the steering angle is increased by  $7.4^\circ$ , and the racing shows a slight understeer. At present, most cars pass through various curves quickly to improve the vehicle handling flexibility, and the steering characteristics are designed to be slightly understeer.

### (3) Scoring evaluation of steady-state slewing test

Due to the small turning radius and track width of the eight-shaped ring project in FSAE racing events, the vehicles participating in the event must have a large lateral acceleration to improve the sensitivity of the racing when turning, to pass through the curve at a higher stable speed. In the evaluation method of automobile industry standards, the lateral acceleration of the neutral steering point is one of the evaluation indicators of the steady-state slewing test [12]. However, the car has



**Fig. 11.** Simulation curve of steady-state rotation test

a slightly understeer characteristic with no neutral point. Based on the evaluation method of automobile industry standard, in this case, the least square method shall be adopted, and the calculation shall be conducted according to the cubic polynomial fitting curve of the variable term. The calculated side acceleration score for neutral steering is full, but cars need a greater side acceleration to improve the race.

Therefore, the maximum lateral acceleration is taken as one of the evaluation indicators of the test. The understeer degree and the body roll degree are scored according to the automobile industry standard, and the comprehensive score is finally calculated.

#### 1. Maximum lateral acceleration score

Calculation formula of maximum lateral acceleration score

$$N_{a_n} = 60 + \frac{40}{a_{100} - a_{60}} (a - a_{60}), \quad (1)$$

where  $N_{a_n}$  is the evaluation score of maximum lateral acceleration,  $a$  is the test value of maximum lateral acceleration;  $a_{60}$ ,  $a_{100}$  are the lower limit and upper limit of maximum lateral acceleration, respectively.

$a_{60}$  and  $a_{100}$  are determined according to previous FSAE racing results,  $a_{60}$  is 0.9 g,  $a_{100}$  is 1.4 g. From Fig. 11a, it can be seen that the maximum lateral acceleration  $a$  is 1.03 g. By substituting each parameter into (1) we obtain the evaluation score  $N_{a_n} = 70.4$  of the maximum lateral acceleration of the steady-state slewing test.

#### 2. Scoring of understeer

The formula for calculating the understeer score is

$$N_U = 60 + \frac{U(U_{60} - U)(\lambda - U)}{U_{100}(U_{60} - U_{100})(\lambda - U_{100})} \times 40, \quad (2)$$

where  $N_U$  is the evaluation score of the understeer degree,  $U$  is the test value of insufficient steering degree,  $\lambda$  is the coefficient calculated by the ratio of  $U_{60}$  to  $U_{100}$ ,  $\lambda = \frac{2 \times U_{60}/U_{100}}{U_{60}/U_{100} - 2}$ ,  $U_{60}$  and  $U_{100}$  are the lower and upper limits of understeer respectively.  $U_{100} = 0.4(^{\circ})/(m/s^2)$ ,  $U_{60} = 1.0(^{\circ})/(m/s^2)$ .

As shown in Fig. 11e, the insufficient steering angle  $U = 0.15(^{\circ})/(m/s^2)$ . Substituting each parameter into (2) yields an evaluation score of  $N_U = 81.8$  for insufficient steering degree.

#### 3. Body roll rating

The calculation formula for car body roll degree score is

$$N_{\phi} = 60 + \frac{40}{K_{\phi60} - K_{\phi100}} \times (K_{\phi60} - K_{\phi}), \quad (3)$$

where  $N_{\phi}$  is the evaluation score of car body roll,  $K_{\phi}$  is the test value of car body inclination,  $K_{\phi60}$  and  $K_{\phi100}$  are the lower and upper limits of the body roll.  $K_{\phi100} = 0.7(^{\circ})/(m/s^2)$ ,  $K_{\phi60} = 1.2(^{\circ})/(m/s^2)$ .

It can be seen from Fig. 11f that the body roll  $K_{\phi}$  is  $0.11(^{\circ})/(m/s^2)$ . Substitute each parameter into (3) to obtain the evaluation score  $N_{\phi} = 147.2$ .

When the evaluation score exceeds 100, the comprehensive score is calculated as 100, so  $N_{\phi} = 100$ .

#### 4. Comprehensive scoring of steady-state slewing test

The formula for calculating the comprehensive score of the steady-state slewing test is

$$N_W = \frac{N_{a_n} + N_U + N_{\phi}}{3}. \quad (4)$$

By substituting each parameter into (4) we obtain the comprehensive score  $N_W = 84.1$  for the steady-state slewing test.

The steady-state slewing simulation curve and test scores show that the body roll score is high, and the understeer degree also meets the requirements. The final score of the steady-state slewing test is 84.1.

#### 4.2. Snake-shaped test

The snake-shaped test, also known as the S-shaped pile winding test, makes the vehicle continuously simulate the serpentine passing through the piles with specified spacing. The test can accurately reflect the handling stability of the racing under continuous sharp turns and near-side slip conditions.

In the high-speed obstacle avoidance project in the FSAE competition, the minimum pile distance is 10 m, which is far less than 30 m in the snake-shaped test pile distance in the national standard. To meet the standard and achieve higher scores in the dynamic project, the pile distance is modified to 10 m, and the speed is the average speed of our formula racing in the high-speed obstacle avoidance project of 45 km/h. Because the distance between the snake-shaped test piles is far lower than the 30 m specified in the national standard, the final comprehensive score of the snake-shaped test is lower than that when the pile distance is 30 m.

##### (1) Serpentine test method

The snake-shaped test consists of 10 stakes to form an obstacle, the stake distance  $L$  is 10 m, and the speed is 45 km/h on average in the high-speed obstacle avoidance project of the Shandong University of Technology formula racing, which includes following the route shown in Fig. 12 to pass through the marking area in a snake-like manner and recording the entire test process.

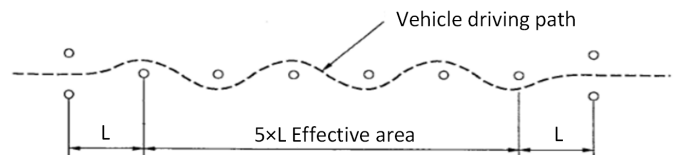
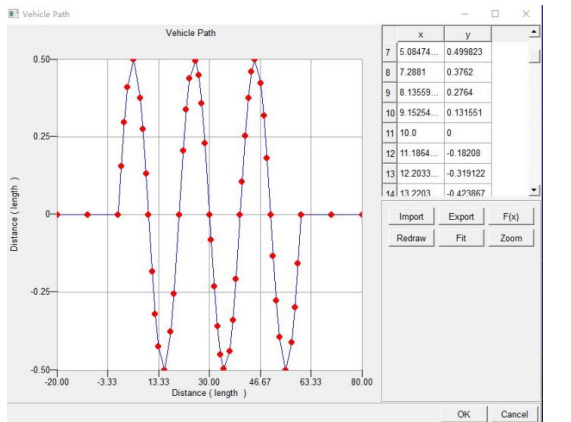


Fig. 12. Layout of serpentine test road piles

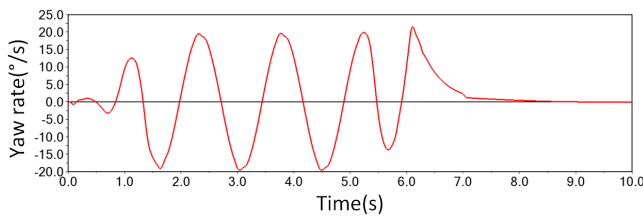
##### (2) Snake-shaped setup and simulation results

In the vehicle simulation of ADAMS/CAR, Event Builder is used to set the track route and the driving events, such as steering, accelerator, braking, etc. according to the test method. The track route is set as shown in Fig. 13a, and the simulation results of the snake-shaped test are shown in Fig. 13b and 13c.

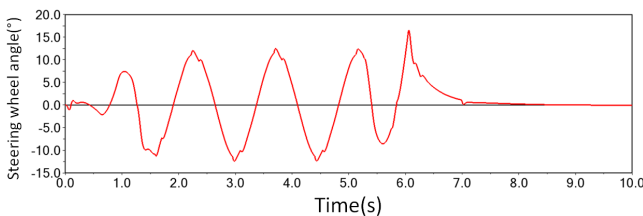
## Handling stability analysis of decoupling suspension for formula racing



(a) Setup of snake-shaped test track route



(b) Yaw rate versus time curve



(c) Change curve of steering wheel angle with time

**Fig. 13.** Simulation diagram of serpentine test

Figure 13c shows that the average steering wheel angle peak  $\theta$  ratio is small at  $11.67^\circ$ . This is because the steering ratio of the steering system is small in racing design, and the maximum single-side steering angle of the steering wheel is only  $134.6^\circ$ . This is designed to give the racing a more flexible turn and allow it to pass faster through the short track.

**(3) Scoring evaluation of serpentine test**

The average yaw rate peak  $r$  and the average steering wheel peak  $\theta$  at the reference speed are scored and finally, the comprehensive score is calculated.

## 1. Average yaw rate peak score

Calculation formula of average yaw rate peak score

$$N_r = 60 + \frac{40}{r_{60} - r_{100}} (r - r), \quad (5)$$

where  $N_r$  is the average yaw rate peak evaluation score,  $r$  is the test value of the average yaw rate peak,  $r_{60}$  and  $r_{100}$  are the

lower and upper limits of the mean yaw rate peak, respectively.  $r_{100} = 10^\circ/\text{s}$ ,  $r_{60} = 25^\circ/\text{s}$ .

From Fig. 13b, the average yaw rate peak value  $r$  is  $19.01^\circ/\text{s}$ . Each parameter is substituted into (5) to obtain the evaluation score  $N_r = 75.97$  of the average yaw rate peak value of the snake-shaped test.

## 2. Average steering wheel angle peak score

Calculation formula of average steering wheel angle peak score

$$N_\theta = 60 + \frac{40}{\theta_{60} - \theta_{100}} (\theta - \theta), \quad (6)$$

where  $N_\theta$  is the evaluation score of the average steering wheel angle peak value,  $\theta$  is the test value of the average steering wheel angle peak value,  $\theta_{60}$  and  $\theta_{100}$  are the lower and upper limits of the average peak steering wheel angle, respectively.  $\theta_{100} = 60^\circ$ ,  $\theta_{60} = 180^\circ$ . In Fig. 13c, it can be seen that the average peak value of the steering wheel angle  $\theta$  is  $11.6^\circ$ . When each parameter is substituted into (6), the evaluation score of the average peak value of the steering wheel angle of the snaking test is  $N_\theta = 116.11$ .

If the evaluation score exceeds 100, the comprehensive score is calculated as 100, so  $N_\theta = 100$ .

## 3. Comprehensive scoring of the serpentine test

The formula for calculating the comprehensive evaluation score of the snake-shaped test is

$$N_S = \frac{2N_r + N_\theta}{3}. \quad (7)$$

Each parameter is substituted into (7) and the comprehensive score of the shaped test is  $N_S = 83.98$ .

It can be seen from the simulation curve and test score of the snake-shaped test that the change range of the yaw rate is relatively small, and the stability and safety of driving can be maintained in case of sharp steering. The average peak value of the steering wheel angle is relatively small, the maneuverability of racing is good, and the steering is flexible in continuous steering. All scores meet the requirements.

**4.3. Comprehensive evaluation of vehicle handling stability**

The calculation formula for the objective evaluation score of manipulation stability is

$$N = \frac{N_W + N_S}{2}. \quad (8)$$

Substitute the evaluation score of each handling stability test into (8) to obtain the comprehensive evaluation score of the vehicle handling stability equal to 84.04, complying with national standards. While the test difficulty is higher than the national standard, the final score is still more than 80 points, which indicates that the vehicle handling stability is good.

## 5. VERIFICATION OF REAL VEHICLE TEST

The decoupling suspension studied in this paper is used in the design and manufacture of the Shandong University of Technology. A real vehicle test was conducted after the racing was manufactured to verify the relevant evaluation indicators of the snake-shaped test and the maximum lateral acceleration reflecting the ultimate lateral performance of the racing. The decoupling suspension race is shown in Fig. 14.

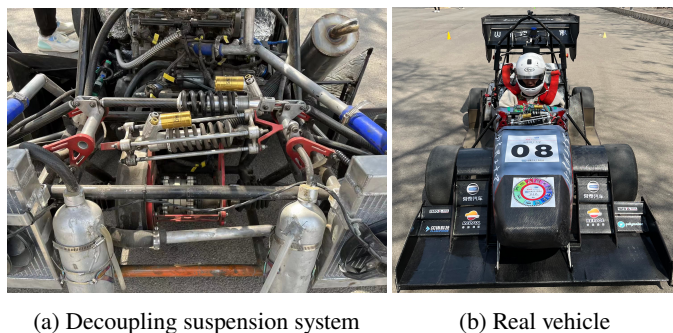


**Fig. 14.** Decoupling suspension racing

This time, the test system is to read the yaw rate data through the MPU-6050 gyroscope, store it in the SD card, and obtain the test process data through the computer. The test system is installed, as shown in Fig. 15.



**Fig. 15.** Installation drawing of test system

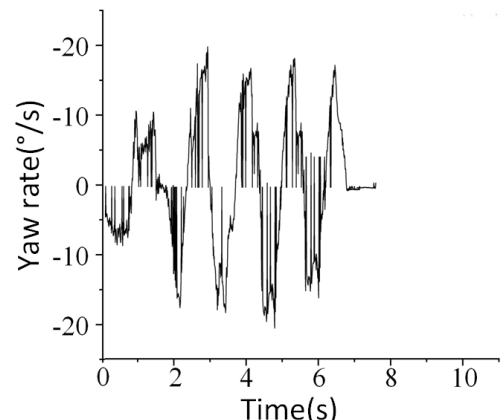
### 5.1. Snake-shaped test

Based on the snake-shaped test method and the use of a pile barrel to form an obstacle, an experienced racer conducted a real vehicle test, and the running of the real vehicle is shown in Fig. 16.

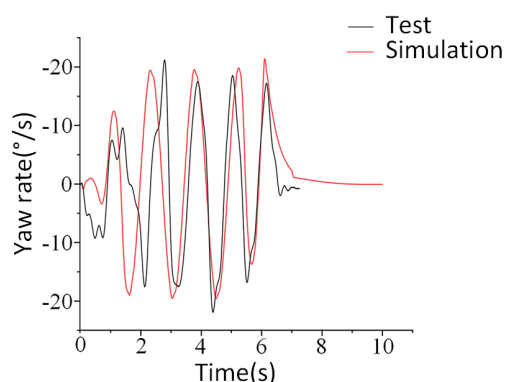


**Fig. 16.** Running of snake-shaped test

At the end of the test, the computer is used to obtain the original data and fit it to get the curve of yaw rate changing with time, as shown in Fig. 17a.



(a) Original data of serpentine test



(b) Yaw rate comparison

**Fig. 17.** Contrast curve of yaw rate between the original data of snake-shaped test and virtual simulation

Due to the influence of sensor error, environment, and other factors during the actual vehicle test, the signal noise will be generated, and some “burrs” will appear on the curve. To improve effective data analysis, the yaw rate comparison curve between the real vehicle test and the virtual simulation is obtained after filtering the original data, as shown in Fig. 17b.

From Fig. 17b it can be concluded that the yaw rate curve of the virtual simulation in the snake-shaped test agrees with the curve obtained by the real car running of the real racer. However, there are some errors between the test and simulation caused by factors such as the long service time of the tire, assembly error, and site pavement, and the error is within the acceptable range.

The test further verifies that the stability of the racing is good, and the racing can have good directional stability under continuous turning conditions.

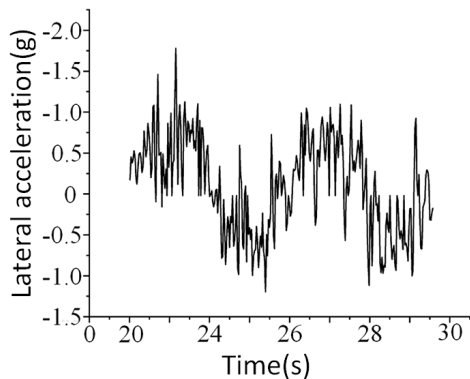
### 5.2. Maximum lateral acceleration test

Because the racing needs a large lateral acceleration to turn quickly, keep the racing running continuously around a 9.125 m radius and observe whether it can maintain a large lateral acceleration during driving. Experienced racers conduct the real car test, and the real car running is shown on Fig. 18.

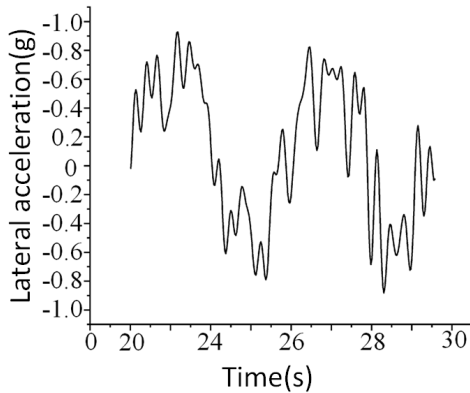


**Fig. 18.** Running of real vehicle

At the end of the test, the original data is acquired by the computer, and the data after the stable driving of the racing is selected to fit and obtain the curve of lateral acceleration with time. The original fitting curve is shown in Fig. 19a, and the filtered curve is shown in Fig. 19b.



(a) Original data of lateral acceleration



(b) Processed lateral acceleration

**Fig. 19.** Curve of lateral acceleration with time

Figure 19b shows that the maximum lateral acceleration of a race can reach 0.91 g during continuous circular driving. This value is slightly lower than the simulation value. Still, the error is within the acceptable range, which is caused by a combination of factors such as long tire use time, assembly error, and ground surface. The ability of the race to last for a long time, around 0.65 g, suggests that the real car can maintain a large continuous lateral acceleration.

The test further verifies that the decoupling suspension system can give the vehicle a large ultimate lateral acceleration, and the riding stability is good.

## 6. CONCLUSIONS

To ensure the decoupling of suspension, a new decoupling arrangement scheme for spring damper assembly is designed in this paper. The rocker arm is transformed into a stepped shaft, and a decoupled suspension model is established. Through kinematic simulation analysis, the decoupled suspension attains the decoupling of pitch stiffness and roll stiffness.

1. In this paper, the maximum lateral acceleration, understeer degree and body roll degree are taken as the evaluation indicators of the test, and the test standard and difficulty are improved to evaluate the vehicle handling stability more comprehensively.
2. The decoupling suspension was applied to the Shandong University of Technology. The test was conducted in a field meeting the competition requirements. The data was read by the MPU-6050 gyro test system and stored in an SD card. The test process data was obtained by a computer and fitted. To improve the effective analysis of data, the original data is filtered. The results show that the yaw angle velocity curve of the virtual simulation in the snake-shaped test is in good agreement with the curve obtained by the real car. The maximum lateral acceleration of the car can reach 0.91 g in continuous circular driving, slightly lower than the simulation value, and the error is within the acceptable range. It is further verified that the decoupling suspension system can make the vehicle have a large ultimate lateral acceleration, and the driving stability of the car is good.

In this paper, there is no in-depth lightweight research on the design of decoupling suspension. Therefore, topology optimization and new materials can be used in the lightweight design of uncoupled suspension to further reduce the suspension mass and improve the vehicle performance.

## REFERENCES

- [1] S. Song, "Joint Study on Aerodynamics and Handling Stability of FSAE Racing Car under Unsteady Wind," M.A. thesis, Jilin University, China, 2021, doi: [10.27162/d.cnki.gjlin.2021.003384](https://doi.org/10.27162/d.cnki.gjlin.2021.003384).
- [2] T.J. Yuen and S.M. Foong, "Ramli R. Optimized suspension kinematic profiles for handling performance using 10-degree-of-freedom vehicle model," *J. Multi-Body Dyn.*, vol. 228, no. 1, pp. 82–99, 2014, doi: [10.1177/1464419313516436](https://doi.org/10.1177/1464419313516436).
- [3] J. Gao and P. Han, "Analysis and optimization of vehicle handling stability with considering front and rear suspension hard point coordinates," *J. Mech. Eng. Sci.*, vol. 236, no. 10, pp. 5318–5341, 2022, doi: [10.1177/09544062211060732](https://doi.org/10.1177/09544062211060732).
- [4] S. Ramakrishna *et al.*, "A Review on Anti-Roll Bar used in Locomotives and Vehicles," *Int. J. Curr. Eng. Technol.*, vol. 7, no. 3, pp. 838–841, 2017.
- [5] J. Zhou and S. He, "Design of third spring decoupling suspension system," *Third International Conference on Control and Intelligent Robotics (ICCIR 2023)*, vol. 12940, pp. 244–251, 2023, doi: [10.11117/12.3011143](https://doi.org/10.11117/12.3011143).
- [6] R. Sindhwan, A. Bhatnagar, and A. Soni, "Design and optimization of suspension for formula Society of Automotive Engineers (FSAE) vehicle," *Mater. Today*, vol. 38, pp. 229–233, 2021, doi: [10.1016/j.matpr.2020.07.077](https://doi.org/10.1016/j.matpr.2020.07.077).

- [7] Y. Kumar, R.A. Siddiqui, Y. Upadhyay, and S. Prajapati, "Kinematic and Structural Analysis of Independent type suspension system with Anti-Roll bar for Formula Student Vehicle," *Mater. Today*, vol. 56, pp. 2672–2679, 2022, doi: [10.1016/j.matpr.2021.09.247](https://doi.org/10.1016/j.matpr.2021.09.247).
- [8] I. Javanshir *et al.*, "Optimization of suspension system of heavy off-road vehicle for stability enhancement using integrated anti-roll bar and coiling spring mechanism," *J. Cent. South Univ.*, vol. 25, no. 9, pp. 2289–2298, 2018, doi: [10.1007/s11771-018-3913-6](https://doi.org/10.1007/s11771-018-3913-6).
- [9] S.S. Kelkar, P. Gautam, S. Sahai, P.S. Agrawal, and R. Manoharan, "A detailed study on design, fabrication, analysis, and testing of the anti-roll bar system for formula student cars," *SN Appl. Sci.*, vol. 3, pp. 1–14, 2021, doi: [10.1007/s42452-021-04279-z](https://doi.org/10.1007/s42452-021-04279-z).
- [10] Ke Ma, "Design and optimization of electric vehicle Air suspension Structure based on handling stability," M.A. thesis, Xihua University, China, 2023, doi: [10.27671/d.cnki.gcjt.2021.000981](https://doi.org/10.27671/d.cnki.gcjt.2021.000981).
- [11] Z. Liu *et al.*, "Suspension Design of Formula Racing Vehicle with Roll Independent Control Function," *Proc. China SAE Congress 2020: Selected Papers. Lecture Notes in Electrical Engineering*, 2022, vol. 769, pp. 35–56, doi: [10.1007/978-981-16-2090-4\\_3](https://doi.org/10.1007/978-981-16-2090-4_3).
- [12] X. Shi, Y. Ye, and Y. Peng, "Pitch Motion Analysis of Front Suspension Based on The Third Spring Structure," *Auto Time*, vol. 08, pp. 79–82, 2020.
- [13] S. Yang *et al.*, "Optimization Analysis of a Decoupling Suspension Based on Adams," *Automob. Appl. Technol.*, vol. 03, pp. 49–54, 2021, doi: [10.16638/j.cnki.1671-7988.2022.003.011](https://doi.org/10.16638/j.cnki.1671-7988.2022.003.011).
- [14] D. Wu, Ning Gao, and Sheng Hong, "Design and Simulation Research on Decoupling Suspension of FSAE Racing Car Based on ADAMS/CAR," *J. Wuhan Univ. Technol.*, vol. 06, pp. 77–84, 2020.
- [15] S. Quan, S. Wei, and F. Fei, "Decoupled Suspension Design and Motion Simulation Analysis of Chines Formula SAE," *Automob. Appl. Technol.*, vol. 15, pp. 59–62, 2024, doi: [10.16638/j.cnki.1671-7988.2024.015.012](https://doi.org/10.16638/j.cnki.1671-7988.2024.015.012).
- [16] Y. Li *et al.*, "The Application of ADAMS Software to Vehicle Handling Stability: A Review," *Perform. Eng. Mainten. Eng.*, vol. 117, pp. 785–795, 2021, doi: [10.1007/978-3-030-99075-6\\_63](https://doi.org/10.1007/978-3-030-99075-6_63).
- [17] A. Pridie and C. Antonya, "The theoretical study of an interconnected suspension system for a formula student car," *Appl. Sci.*, vol. 11, no. 12, pp. 5507, 2021, doi: [10.3390/app11125507](https://doi.org/10.3390/app11125507).
- [18] L. Zhang *et al.*, "Multi-objective optimization study of vehicle suspension based on minimum time handling and stability," *Proc. Inst. Mech. Eng. Part D-J. Automob. Eng.*, vol. 234, no. 9, pp. 2355–2363, 2020, doi: [10.1177/0954407020909663](https://doi.org/10.1177/0954407020909663).
- [19] B.M. Kim, J.W. Kim, I.D. Moon, and Ch.Y. Oh, "Optimal combination of design parameters for improving the kinematics characteristics of a midsize truck through design of experiment," *J. Mech. Sci. Technol.*, vol. 28, no. 3, pp. 963–969, 2014, doi: [10.1007/s12206-013-1167-7](https://doi.org/10.1007/s12206-013-1167-7).
- [20] T. Vlad and C. Alexandru, "Multi-Criteria optimization of an innovative suspension system for race cars," *Appl. Sci.*, vol. 11, no. 9, pp. 4167, 2021, doi: [10.3390/app11094167](https://doi.org/10.3390/app11094167).
- [21] Z. Zhang *et al.*, "Joint Research on Aerodynamic Characteristics and Handling Stability of Racing Car under Different Body Attitudes," *Energies*, vol. 15, no. 1, p. 393, 2022, doi: [10.3390/en15010393](https://doi.org/10.3390/en15010393).
- [22] M. Balena, G. Mantriota, and G. Reina, "Dynamic handling characterization and Set-Up optimization for a Formula SAE race car via Multi-Body simulation," *Machines*, vol. 9, no. 6, p. 126, 2021, doi: [10.3390/machines9060126](https://doi.org/10.3390/machines9060126).
- [23] Standards of the People's Republic of China. 2014. GB/T6326-2014 Automobile Handling Stability Test Method.
- [24] Standards of the People's Republic of China. 1999. QC/T 480-1999 Limits and Evaluation Methods of Automobile Handling Stability Index.
- [25] Y. Chai, "Simulation Optimization and Evaluation of FSAE Racing Suspension Based on Adams," M.A. thesis, North University of China, China, 2020, doi: [10.27470/d.cnki.ghbgc.2020.000790](https://doi.org/10.27470/d.cnki.ghbgc.2020.000790).
- [26] H. Zhang, "Handling Stability Optimization of FSEC Racing Suspension Based on Virtual Prototype Technology," M.A. thesis, Yangzhou University, China, 2022, doi: [10.27441/d.cnki.gyzdu.2022.000541](https://doi.org/10.27441/d.cnki.gyzdu.2022.000541).
- [27] D. Zhou, "FSAE Racing Car Layout, Suspension Design and Handling Stability Analysis," M.A. thesis, Chang'an University, China, 2013.
- [28] J. Qiao *et al.*, "Simulation of FSAE Racing Car Control Stability," *Beijing Automot. Eng.*, vol. 4, pp. 7–9+20, 2023, doi: [10.14175/j.issn.1002-4581.2023.04.002](https://doi.org/10.14175/j.issn.1002-4581.2023.04.002).
- [29] C. Yang, "Research on Modeling and Optimal Design of Double Wishbone Front Suspension System for Baja Racing Car," M.A. thesis, Chongqing Jiaotong University, China, 2021, doi: [10.27671/d.cnki.gcjt.2021.000981](https://doi.org/10.27671/d.cnki.gcjt.2021.000981).
- [30] C. Hong, "Tire Model Parameter Identification and Vehicle Handling Stability Simulation Analysis of Formula Student Racing Car," M.A. thesis, Chang'an University, China, 2019.
- [31] H. Cheng, B. Wu, and D. He, "Optimization Design of Suspension and Steering System for FSAE Racing Car," *J. Eng. Mech. Mach.*, vol. 8, pp. 67–81, 2023, doi: [10.23977/jemm.2023.080108](https://doi.org/10.23977/jemm.2023.080108).